ORIGINAL PAPER



Insight into the Viscous and Adhesive Contributions to Hydrogel Friction

Tooba Shoaib^{1,2} · Rosa M. Espinosa-Marzal¹

Received: 14 March 2018 / Accepted: 19 June 2018 / Published online: 29 June 2018 © Springer Science+Business Media, LLC, part of Springer Nature 2018

Abstract

Investigation of the mechanisms underlying hydrogel lubrication is pivotal in understanding the complexity of biolubrication. In this work, the frictional characteristics of poly(acrylamide) hydrogels with varying composition have been studied over a wide range of sliding velocities and normal loads by colloidal probe lateral force microscopy. The results show that the friction force between the hydrogel and the colloid increases with velocity at sliding velocities above a transition value (V^*) , while the friction force at slower sliding velocities depends on the composition, and it can either increase or decrease with velocity. Based on the viscoelastic behavior of hydrogels, we model hydrogel friction as the combination of viscous dissipation and the energy dissipated through the rupture of the transient adhesive bridges across the interface. The model parameters depend on relaxation characteristics of the confined polymer network at the interface and on the (bulk) viscoelastic behavior of the hydrogel and are sensitive to the compressive stress. We observe a collapse of the experimental data (at different loads and velocities and for hydrogels with different compositions) in a non-monotonic master curve with a minimum friction force at the transition velocity. Furthermore, a simple relation for the transition velocity V^* is derived from theory, thereby demonstrating the competing effect of both the adhesive and the viscous contributions to friction, which helps to reconcile discrepancies between previous studies of hydrogel friction.

Keywords Hydrogels · Soft matter lubrication · Lateral force microscopy · Friction

1 Introduction

Tribosystems found in nature, including the respiratory and gastrointestinal tracts, the oral cavity, and the eye, are predominantly lubricated by mucous gel layers; they operate efficiently with a water-based lubricant and are characterized by low coefficients of friction and wear rates [1–6]. Mucous typically consists of networks of proteins and polysaccharides that encompass a large amount of water and respond

Electronic supplementary material The online version of this article (https://doi.org/10.1007/s11249-018-1045-7) contains supplementary material, which is available to authorized users.

- ⊠ Rosa M. Espinosa-Marzal rosae@illinois.edu
- Department of Civil and Environmental Engineering, University of Illinois at Urbana—Champaign, 205 North Matthews Avenue, Urbana, IL 61801, USA
- Department of Materials Science and Engineering, University of Illinois at Urbana—Champaign, 1304 West Green Street, Urbana, IL 61801, USA

to external normal and shear forces, so as to protect the underlying tissues from incurring any damage [7]. Because of their semblance to these mucous layers, hydrogels often serve as model systems to understand biolubrication. Hydrogels are biphasic materials composed of a polymer network and large amounts of water, which renders them soft, viscoelastic—reflecting the intrinsic viscoelasticity of the polymer network—and poroelastic, as a result of the flow of the interstitial fluid. Further, their biocompatibility makes hydrogels very promising as biomaterials for targeted medical applications, which has increased the interest in investigating hydrogel's frictional characteristics [3–6].

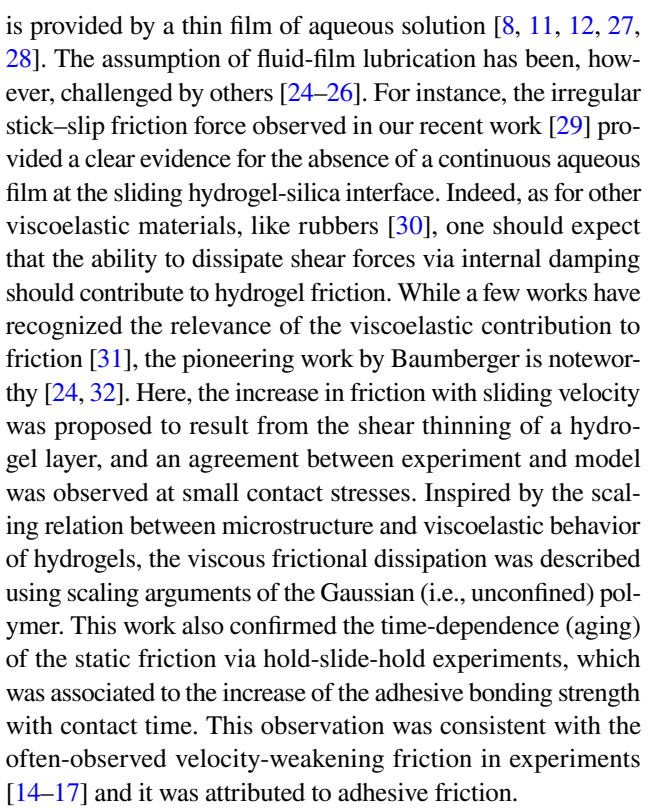
Numerous studies have experimentally explored the load and speed dependence of the frictional response of hydrogels and have showed often a deviation from Amonton's law. The reported effects of the load on friction are disparate, ranging from an increase of friction with load [8], a load-independent friction force [9], and even a decrease in friction with increase in load [10, 11], perhaps as a result of the increase in surface conformity. Regarding the influence of the velocity, friction coefficients of poly(vinyl alcohol) hydrogels



against a hard and impermeable counter-surface decreased with the sliding velocity [8, 11, 12], while an opposite trend was observed for poly(N-isopropylacrylamide) [10]. The different trends of friction with velocity were attributed to the slow dynamics of the polymer. For instance, for poly(N-isopropylacrylamide) hydrogels, long contact times (slow sliding) enable the polymers to disentangle in response to the applied shear, while with increasing velocities, there is no sufficient time for disentanglement to occur and stretching and rupture of the adhesive bonds across the interface occur, thereby causing an increase in the dissipated energy. The poroelastic response of hydrogels has been also associated to velocity-dependent changes in hydrogel friction more recently [13].

Comprehensive experiments by Gong et al. have helped to reconcile the seemingly contradictory velocity dependence of the frictional response, since they demonstrated the nonmonotonic trend of the friction force, first increasing (i.e., velocity-strengthening) and then decreasing (i.e., velocityweakening) with sliding velocity [14–17]. Furthermore, it was reported that, after a minimum was achieved at a socalled critical velocity V_c , friction increased with velocity, which was associated to elastohydrodynamic lubrication [15]. Below the critical velocity V_c , hydrogel friction was described in the context of Schallamach's model for rubber friction [18]. Here, the adhesive friction is originated by the interplay between formation and rupture of adhesive and reversible molecular bonds across the interface, being both thermally activated processes, yet affected by the shear force. According to this model, friction results from the energy dissipated when these bonds are broken. The fluctuation length (ξ) and relaxation times for polymer attachment and detachment were used to describe the adhesive component of friction [14]. The so-called adsorption-desorption model used scaling arguments to define the critical velocity, $V_c = k_B T / \eta \xi^2$, based on the relaxation characteristics of the free (unconfined) polymer [15, 19], T being the temperature, $k_{\rm B}$ the Boltzman constant, and η the viscosity of the solvent. This model is powerful in *qualitatively* describing many reported experimental results. For example, friction can be modulated by varying the adhesion to the counter-surface, which can be increased through the collapse of the gels in a poor solvent [10, 20], via a greater crosslinking degree [19, 21-23] or through changes of the monomer chemical composition [12]. Nevertheless, the quantitative comparison of the model to experimental results has been very limited [14], and recent works have emphasized the lack of quantitative agreement, including the deviation from the predicted critical velocity, V_c [24–26].

Several studies have attributed the increase in hydrogel friction with sliding velocity (above $V_{\rm c}$) to hydrodynamic lubrication, thereby presuming the absence of contact between the counter-surfaces, and thus, assuming that hydrogel lubrication



Although appreciable consensus exists behind the peculiar dependencies of hydrogel friction on load and velocity, a prediction of the behavior based on hydrogel microstructure and underlying mechanisms is still not possible, which emphasizes the gap in the fundamental knowledge. The present work emphasizes that friction results from the interplay of viscous and adhesive frictional dissipation. We present friction-force measurements as a function of the sliding velocity spanning four orders of magnitude and over a wide range of applied loads for three hydrogels, which enables us to quantitatively evaluate the mechanisms underlying the frictional response. The fit of the viscous–adhesive model to the experimental results provides the bulk and interfacial properties that dictate friction. Importantly, it is shown that the confinement imposed by the counter-surface not contemplated in the previously proposed scaling approaches affects the relaxation characteristics of the polymer network at all sliding velocities, and thereby, the frictional behavior of hydrogels. Furthermore, the experimental data collapse in a master curve through appropriate scaling of friction and sliding velocity based on the key material properties that dictate friction.

2 Materials and Methods

Polyacrylamide (PAAm) hydrogels with three different compositions were prepared by mixing varying concentrations of acrylamide (monomer), bis-acrylamide (crosslinker)



Tribology Letters (2018) 66:96 Page 3 of 14 **96**

and DI water following the protocol in Reference [33]. The hydrogels are referred here as 4, 6, and 12% hydrogels for concentrations of the acrylamide monomer of 4.4, 6.4, and 12.4 wt%, respectively. The weight percentages of monomer, crosslinker, and water are given in Table S1. The detailed protocol of the silane treatment of coverslips (to render them hydrophilic and well grafted to the hydrogel) and of the glass slides (to render them hydrophobic) is described in our previous work [29]. Solutions of monomer, crosslinker, and water were degassed for 15 min and polymerized via the addition of an initiator (ammonium persulfate) and an accelerator (tetramethylethylenediamine), each at a concentration of 1/100 of the total volume. 800 µl of precursor solution was pipetted on the hydrophobic glass slide and sandwiched between the glass slide and the hydrophilic coverslip to yield a hydrogel thickness (H) of ~2 mm. After 30 min of gelation, the coverslip with the hydrogel was removed from the hydrophobic glass slide, rinsed with DI water, and then stored in DI water at 4 °C for 1 day. All chemicals were purchased from Sigma Aldrich (USA).

Indentation and friction-force measurements were conducted with an atomic force microscope (Nanowizard Ultra, JPK Instruments, Germany). Silica beads with two diameters, 20 µm (Duke Scientific, Thermo Scientific, CA, USA) and 5 µm (Microspheres-Nanospheres, USA), were attached to the end of tipless cantilevers (nominal spring constant = 0.4 N/m, CSC37-No Al/tipless, Mikromash, USA) using an epoxy glue (JB-Weld, Sulphur Springs, TX, USA). Before attaching the colloids, the normal stiffness of the cantilevers was determined by the thermal noise method and the lateral stiffness was obtained by means of the wall calibration method [34]. The AFM cantilevers were cleaned in an ethanol bath followed by UV ozone for 30 min just before the AFM experiment. RMS roughness of each silica colloid within the area of contact with the hydrogel was determined via reverse imaging using a clean test grating (MikroMasch, Spain) and was smaller than 5 nm.

Indentation tests were conducted on each hydrogel sample prior to the friction-force measurements. The measurements were conducted at an approach/retraction velocity of 2 μ m/s. The JKR model was used to determine simultaneously the elastic modulus and the surface energy of the hydrogels. Using a computation software (Wolfram Mathematica version 11.0.0.0), the unloading curves were fit to

$$h = h_{c} + \frac{a^{2}}{3R} + \frac{F}{2aE^{*}}$$

$$a^{3} = \frac{3R}{\left(4E^{*}\right)} \left(F + 3\pi\gamma R + \left(6\pi\gamma RF + (3\pi\gamma R)^{2}\right)^{\frac{1}{2}}\right)$$
(1)

F being the indentation force, h the indentation depth, $h_{\rm c}$ the contact point, R the colloid radius, a the contact radius,

 γ the surface energy, and E^* the contact modulus. Inertia and hydrodynamic forces were estimated to be negligible at the selected conditions. The contact modulus is defined by $1/E^* = (1 - v_{\rm gel}^2)/E_{\rm gel} + (1 - v_{\rm sil}^2)/E_{\rm sil}$, where E is the elastic modulus and v the Poisson's ratio of the hydrogel ($v_{\rm gel} = 0.45$) and silica colloid ($v_{\rm sil} = 0.168$ and $E_{\rm sil} = 72.2$ GPa [35]), respectively.

To ensure elastic response, the fits were limited to indentation depths smaller than $h \sim 0.35 \, \mu m$. This results in a/R and h/H ratios of less than 0.3 and 0.1, respectively, and hence, the assumption of small deformation and negligible substrate effects that is required for the use of the JKR model holds well [36]. Nevertheless, the elastic modulus remained unmodified when fitting the entire indentation curve in the range of selected loads ($\leq 50 \, nN$).

Friction-force measurements were performed at varying normal loads in the range of 5–50 nN with sliding velocities spanning over four orders of magnitude in the range of 0.5–500 μ m/s. The sliding distance was selected to be 29 μ m (i.e., larger than the colloid radii, 2.5 and 10 μ m, respectively) to ensure sliding of the colloids on the hydrogels [37], which was confirmed through the inspection of the lateral force. At least 8 lateral force loops at each load were measured by recording the lateral deflection of the cantilever tip in the forward (trace) and reverse (retrace) directions. The friction force was calculated by averaging over the half width of the trace and retrace scans in each loop.

3 Experimental Results

A prominent hysteresis was measured between loading and unloading indentation curves with large work of adhesion on unloading (not shown). The elastic modulus and the surface energy of the hydrogels were obtained by using the JKR model to fit the unloading indentation curves. Figure 1a shows results for selected 4, 6, and 12% hydrogel samples, for which average elastic moduli were found to be 2.3 ± 0.9 , 6.8 ± 0.9 , and 18.6 ± 3.1 kPa, respectively. These values are in good agreement with previously reported elastic moduli of polyacrylamide hydrogels with similar composition [38, 39]. As shown in Fig. 1b, the surface energy is largest for the 6% hydrogels, which indicates that the combination of a higher polymer concentration (compared to the 4% hydrogels) and a smaller crosslinker concentration (compared to 12% hydrogels) favors the adhesion to the colloid surface. The smaller crosslinker concentration is expected to enhance the mobility of the polymer network thereby enabling the matrix to conform better to the colloid. Although the trends of elastic modulus and surface energy were consistent across the synthesized samples with the same polymer concentration, the values varied, and hence, they were determined



96 Page 4 of 14 Tribology Letters (2018) 66:96

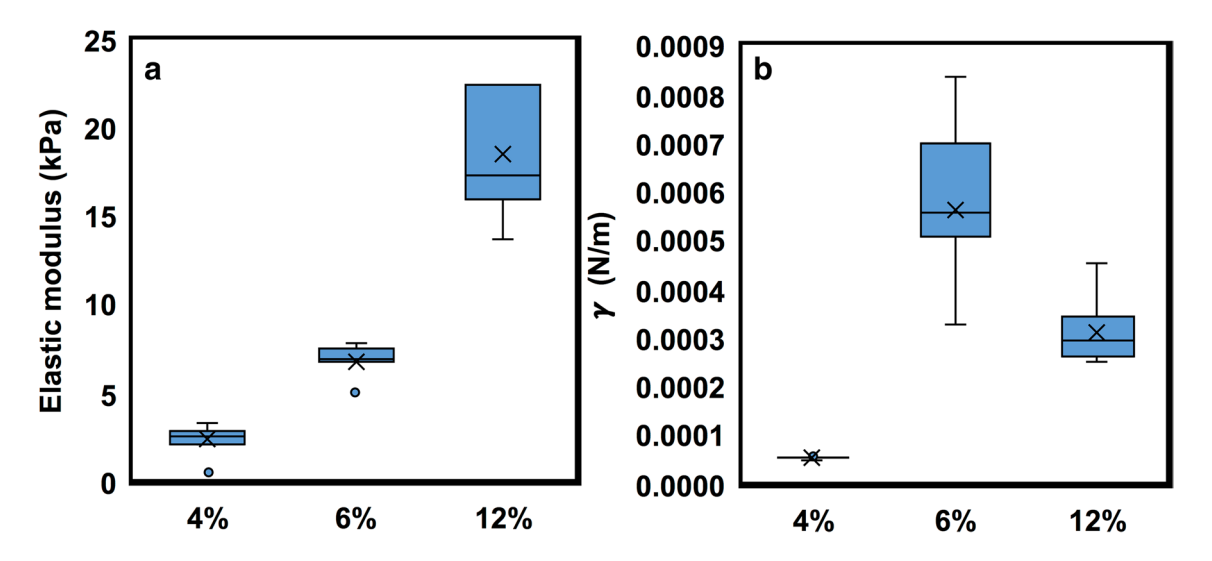


Fig. 1 a Elastic modulus and **b** surface energy (γ) of representative 4, 6, and 12% hydrogels obtained by fitting the JKR model to the indentation (unloading) curves. The box diagrams show the mean (middle line), average (cross), 25 and 75% quartiles, outliers if present (circles) and standard deviation of the elastic modulus and the

surface energy. The Hertzian contact mechanics model was also fit to the loading force-indentation curves, which led to elastic moduli in good agreement with those obtained using the JKR model. Colloid radius = $20 \, \mu m$. Indentation rate = $2 \, \mu m/s$. Spring constant = $0.5 \, N/m$

for each single sample where friction was measured. The corresponding values of the elastic moduli are given in the following diagrams.

Figure 2a–c shows representative friction-force measurements for 4, 6, and 12% hydrogels as a function of the velocity and at different normal loads (see color legend in Fig. 2a). A different velocity dependence of the friction force is observed as a function of the polymer concentration; note that results for different hydrogels are shown in the Supplementary Information (SI, Fig. S1) to illustrate

the variability across hydrogels synthesized following the same protocol. Friction decreases with sliding velocity for 4%-PAAm hydrogels, while it increases with sliding velocity for 12% hydrogels, thereby exhibiting clear velocity-weakening (i.e., decrease in friction with increasing velocity) and strengthening frictional responses (i.e., increase in friction with increasing velocity), respectively. In the case of 6%-PAAm hydrogels, a transition from a velocity-weakening to a velocity-strengthening behavior was often observed (Fig. 2b). It is to be noted that the increase of friction with

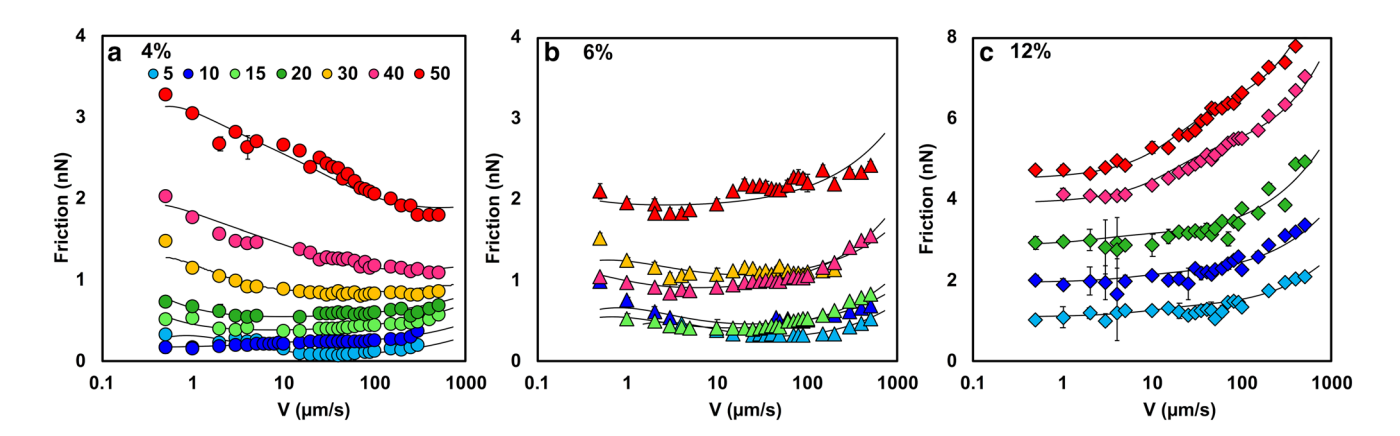


Fig. 2 Friction force as a function of the sliding velocity for **a** 4% (circles), **b** 6% (triangles), and **c** 12% (diamonds) PAAm hydrogels at following normal loads: 5 (light blue), 10 (dark blue), 15 (light green), 20 (dark green), 30 (yellow), 40 (fuchsia), and 50 (red) nN. The elastic moduli of the three hydrogels are **a** 1.8 ± 0.9 , **b** 9.9 ± 0.2 , and **c** 12.9 ± 1.3 kPa, respectively. At least 4 loops were used to calculate the friction force. There is a quantitative agreement between

consecutive loops, which is reflected in the small error bars (often smaller than the symbol size and therefore not visible), indicating that the hydrogel deformation is reversible, i.e., the hydrogel fully recovers during the measurement of each loop. The black lines give the calculated friction force according to the viscous–adhesive model (Eqs. 2–5). Colloid diameter = $20 \mu m$. Spring constant = 0.4 N/m. Note the different scales on the *Y*-axis of (c). (Color figure online)



Tribology Letters (2018) 66:96 Page 5 of 14 **9**6

applied normal load is not always obvious (see e.g., Fig. 2b, under applied loads of 30 and 40 nN), which is mainly attributed to the concurrent influence of load and velocity on the friction force.

While 4 and 12% hydrogels show a consistent behavior across samples, the behavior of 6% hydrogels showed certain variability, i.e., different trends of the friction force were observed as a function of the velocity (see Fig. S1b). Such variable response of 6% hydrogels is attributed to the transitional nature of their frictional characteristics, reflected in the prominent minimum in friction at an intermediate velocity (Fig. 2b). Friction-force measurements across different 6% hydrogel samples demonstrated that a lower elastic modulus leads to a more prominent velocity-weakening regime, which is consistent with the frictional characteristics of the 4%-hydrogels (see e.g., Fig. S1b for ~5 kPa). Nevertheless, the results shown in Fig. 2b are more representative of 6% hydrogels.

Friction was also measured with 5-µm colloids and representative experimental results are shown in Fig. 3. Here, a minimum in the friction force is reproducibly observed for the three hydrogels, i.e., a transition from a velocity-weakening to a velocity-strengthening frictional response. Although the loads applied with 5- and 20-µm colloids were the same, the use of a smaller colloid results in higher contact stresses at the same applied loads, and thereby, it leads to a more prominent squeeze-out of the interstitial water, as justified later (see calculated contact stresses in Table S2 in the SI).

Figure 4 shows representative measurements of the lateral force as a function of the sliding distance. Only 10 μ m of the total sliding distance (29 μ m) are shown here to illustrate the lateral force at the turning point, when the velocity of the cantilever changes from zero to 1 μ m/s at a constant load of 40 nN. For the three selected hydrogels, there is an initial increase of the lateral force over a distance of

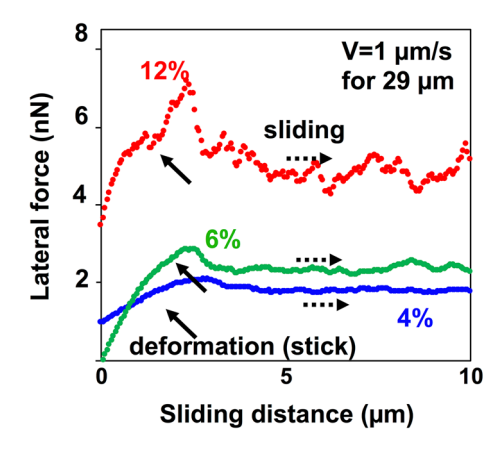


Fig. 4 Lateral force as a function of the sliding distance for three selected hydrogels with elastic moduli of 1.8 (0.1) (blue, 4% hydrogel), 4.9 (0.2) (green, 6% hydrogel), and 12.9 (1.3) kPa (red, 12% hydrogel), respectively, at the sliding velocity of 1 μ m/s and a load of 40 nN. Only the initial 10 μ m of the total stroke length are shown to illustrate the stick period (full arrow) versus sliding (dashed arrow). Colloid diameter: 20 μ m. (Color figure online)

~2 µm, before the force decreases and achieves a plateau. The recorded height of the cantilever demonstrates that this change in the lateral deflection of the cantilever is not originated by the surface topography, which excludes pile-up of the hydrogel. Instead, the increase in the lateral deflection arises from static friction between the hydrogel and the colloid. On applying a tangential force, the near-surface region of the hydrogel deforms more than the bulk, and when the energy stored overcomes the work of adhesion, the colloid starts sliding. Similar results were observed under other conditions, with more or less pronounced increase in lateral force (stick) depending on load and polymer concentration. Since the sliding distance was selected to be much larger

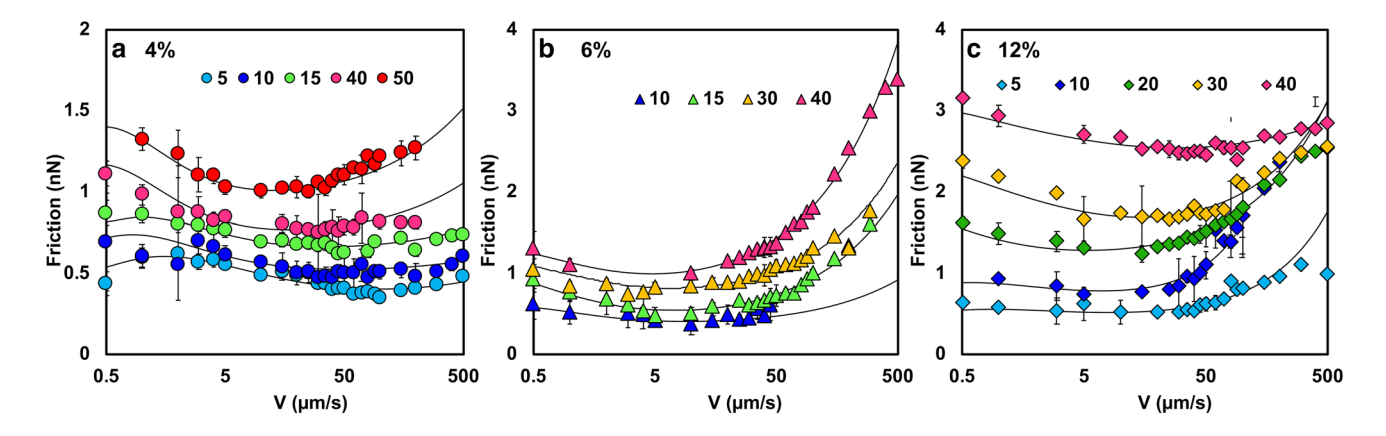


Fig. 3 Friction force as a function of the sliding velocity for **a** 4% (circles), **b** 6% (triangles), and **c** 12% (diamonds) PAAm hydrogels at following normal loads: 5 (light blue), 10 (dark blue), 15 (light green), 20 (dark green), 30 (yellow), 40 (fuchsia), and 50 (red) nN. The elastic moduli of the three hydrogels are **a** 2.34 ± 0.3 **b**

 14.9 ± 0.9 , and c 17.5 ± 0.5 kPa. At least 4 loops were used to calculate the friction force. The black lines give the calculated friction force according to the viscous-adhesive model (Eqs. 2–5). Colloid diameter=5 μ m. Spring constant=0.36 N/m. (Color figure online)



96 Page 6 of 14 Tribology Letters (2018) 66:96

than the stick length, and the friction force (i.e., the half loop width) was only calculated during the sliding period, the experimental results in Figs. 2 and 3 and S1 only reflect the steady-state kinetic friction.

4 Model for Viscous and Adhesive Hydrogel Friction

The proposed model to quantify hydrogel friction considers the superposition of an adhesive and a viscous friction force. The adhesive contribution to friction is based on the theory originally developed by Schallamach for rubber friction [30, 40], which can be applied to any adhesive sheared interface bridged together by reversible, adhesive bonds. The present model, however, differs from previous approaches because it considers the effect of load on polymer relaxation; therefore, we refrain from using simplified scaling arguments, which neglect this phenomenon. The viscous contribution to friction originates from the deformation of a near-surface hydrogel region of μm -thickness, which is shown to exhibit shear-thinning behavior.

The colloid interacts with the hydrogel through a number (N) of transient adhesive bonds (so-called bridges or junctions [41]), which determine the adhesive contact area $A_{\rm b} = N \cdot \Delta$, each junction of area Δ . These junctions form and are stretched in the lateral direction until the polymer detaches from the colloid and relaxes to its equilibrium state, while other junctions form simultaneously in an incoherent manner. Each junction is characterized by thermal activation energies of formation $\Delta E_{\rm f}$ and rupture $\Delta E_{\rm r}$; detachment occurs either by thermal excitation or by an external shear force. The mean time of bond rupture depends on ΔE_r according to $\tau_0 \sim \tau^* \exp(\Delta E_r/kT)$, and it is reduced by the applied lateral force, $\tau_r = \tau_0 \exp(-(f \cdot l_a)/kT)$, where f is the lateral force acting on each junction and l_a is a shearactivated length of molecular dimensions [40]. The rupture of bonds can also happen when a critical deformation of the junction or yield length (l^*) is reached [41]. The transient bonds reform after a characteristic mean time according to $\tau_{\rm f} \sim \tau^* \exp(\Delta E_{\rm f}/kT)$. The fluctuation time of the polymer, τ^* , can be larger than under unconfined conditions due to the confinement imposed by the counter-surface [42] and to large deformations [43], thereby differing from predictions according to Gaussian elasticity, $\tau^{\rm u} \sim \eta \xi^3/k_{\rm B}T$ [44].

The adhesive friction force $F_{\rm adh}$ is thus given by the elastic force of each junction f multiplied by the number of junctions in adhesive state N. According to Reference [41], an analytical expression can be derived to describe the adhesive friction in the context of Schallamach's model, if it is assumed that the lateral force does not decrease the energy barrier for bond rupture. As justified in the SI, this approximation ($\tau_{\rm r} = \tau_0$). is acceptable for hydrogels because the lateral force is very

small. The simplified expression for the adhesive component of friction (see the derivation in the SI) is given by

$$F_{\text{adh}} = Nf = N\frac{\Delta GVt}{d} = \frac{A_bGVt}{d}$$

$$\sim \frac{A_bGV\tau_0}{d} \frac{\left(1 - \left(1 + \frac{l^*}{V\tau_0}\right) \exp\left(-\frac{l^*}{V\tau_0}\right)\right)}{1 - \exp\left(-\frac{l^*}{V\tau_0}\right)}$$
(2)

G being the shear modulus, d the thickness of the junction, Vt/d the strain of the adhesive bridge, and t the time elapsed since the zero-state stress, which considers the probability of formation and rupture of junctions. The adhesive contact area, $A_{\rm b}$, is estimated as $A_{\rm b} = A_{\rm V} t_{\rm b}/(t_{\rm b} + \tau_{\rm f})$, $A_{\rm V}$ being the contact area during sliding, and $t_{\rm h}$ the mean life time of the adhesive junctions, $t_b = \tau_0 (1 - \exp(-l^*/V\tau_0))$, which accounts for the probability of a junction to stay in an adhesive state. Thus, the adhesive friction force depends on G, d and on microscopic characteristics of the polymer network at the contact, l^* , τ_0 and $\tau_{\rm f}$. Equation (2) predicts that friction increases with velocity at low sliding velocities owing to the increasing elongation of each junction with speed (Vt), while the rupture of the adhesive bonds is increasingly promoted with greater velocities but at a lesser rate so that the friction force increases with velocity, approximately in a logarithmic fashion. At high velocities, as only a few bonds can form simultaneously, friction is mainly dictated by the rate of bond formation, $1/\tau_f$, thereby yielding a velocity-weakening mechanism for the friction force. The competition between bond rupture and formation leads to a peak or a plateau of the friction force over an intermediate velocity range. Figure S2 in the SI illustrates the influence of various parameters on F_{adh} .

The failure of this theory to predict sliding friction of rubbers at very slow velocities was recognized by Schallamach [18]. The adhesive friction did not tend to zero by decreasing the velocity as expected from Eq. (2), but instead, a *quasi*-velocity independent friction value (F_0) was observed in experiments [30], which was associated to static friction [18, 45]. Indeed, the hydrogel-glass interfacial strength has been also observed to age (increase) logarithmically with contact time, which was attributed to the slow increasing number of adhesive bonds with time [24]. As shown in Fig. 4, static friction is also present at the hydrogel-colloid interface, which suggests that a (quasi)-velocity independent term (F_0) might be needed to describe hydrogel friction at slow sliding velocities more precisely.

Inspired by previous attempts to describe the friction force of contacts lubricated by polymer melts [46], we propose to model the viscous component of friction as a viscous force assuming a Couette flow of a hydrogel film with an effective viscosity $\eta_{\rm eff}$:

$$F_{\rm vis} \sim \frac{16}{5} A_{\rm V} \eta_{\rm eff} \frac{V}{\delta} \log \left(\frac{2R}{\delta}\right)$$
 (3)



Tribology Letters (2018) 66:96 Page 7 of 14 **96**

where δ is the thickness of the sheared film. Equation (3) is strictly valid for a sphere-plane geometry with $R\gg\delta$, while the most common relation, $F_{\rm vis}\sim A_{\rm V}\eta_{\rm eff}V/\delta$ is only valid for plane-plane geometries. The effective viscosity $\eta_{\rm eff}$ is described according to $\eta_{\rm eff}\sim\eta_0\dot{\gamma}^n=\eta_0(V/\delta)^n$, which accounts for Newtonian (n=1) and non-Newtonian behavior $(n\neq1)$ of the hydrogel film.

At applied pressures smaller than the osmotic pressure of the hydrogel [47] (Π), a time-dependent response arises from the rearrangements of the polymer network [47]. If the applied pressure is, however, larger than Π , the solvent is squeezed out and the poroelastic response of the hydrogel influences the time-dependent contact area [48, 49]. The contact stress in our experiments (Table S2) may be larger than the osmotic pressure, as described later, and hence, we cannot exclude that fluid drainage happens. The migrating contact area A_V (the subindex V indicates a sliding contact) thus differs from the static contact area $(A_0$, where the subindex 0 indicates the contact at a sliding velocity V=0, i.e., upon indentation) at the same applied load as a result of the time-dependent deformation. In the limit of small deformations [50, 51], the sliding contact radius $a_{\rm V}$ can be roughly approximated as

$$a_{\rm V}^2 \sim R \delta_{\rm V} = a_0^2 \frac{\delta_{\rm V}}{\delta_0} = a_0^2 \frac{\delta^{`}(1 - \exp(-t^{`}_{\rm V}/\tau_{\rm PV}))}{\delta^{`}(1 - \exp(-t^{`}_{\rm O}/\tau_{\rm PO}))}.$$

 $au_{\rm P}$ being the relaxation time of the hydrogel (due to fluid drainage and/or to rearrangements of the polymer network) with an effective diffusivity $D\left(\tau_{\rm PV}\sim a_{\rm V}^2/D\right)$ and $\tau_{\rm PO}\sim a_{\rm O}^2/D$, assuming D to be the same for the static and migrating contact areas) and t' the contact time ($t'_0=\delta_0/\dot{\delta}_0$ and $t'_{\rm V}=a_{\rm V}/V$). The indentation depths, $\delta_{\rm V}$ and δ_0 , are described according to a Kelvin-Voigt model, which has been shown to be appropriate for polyacrylamide hydrogels [52]. The linearization of this expression yields

$$a_{\rm V}^2 \sim a_0^2 \frac{t_V'/\tau_{PV}}{t_0'/\tau_{P0}} = a_0^2 \frac{R\dot{\delta}_0}{Va_v}$$

And after rearranging, the velocity-dependent contact radius a_V and area A_V are approximated as

$$\begin{split} a_{\rm V} &\sim \left(\frac{a_0^2 \dot{\delta}_0 R}{V}\right)^{1/3} \\ A_{\rm V} &= \pi \left(a_{\rm V}^2 + \delta_{\rm V}^2\right). \end{split} \tag{4}$$

Figure S3 illustrates the significant change of the contact area as a function of velocity and load according to Eq. (4). It should be noted that Eq. (4) is only valid in the limit of small deformations $(R >> \delta)$ and after linearization of the indentation depth $(\delta_v \text{ and } \delta_0)$, and hence, deviations

of our experimental results from the model are obviously expected. A precise estimation of the sliding contact area would require solving a contact mechanics problem coupled with flow mechanics using appropriate finite element modeling for large deformations and additional consideration of the viscoelasticity of the polymer network, which is out of the scope of this work.

The total friction force results from the addition of the adhesive and viscous contributions and the static friction:

$$F = F_0 + F_{\text{adh}} + F_{\text{vis}}. ag{5}$$

4.1 Fitting Procedure

The JKR model was used to calculate the static contact radius a_0 and the indentation depth δ_0 as a function of the normal load using the elastic modulus and surface energy of the hydrogels, and Eq. (4) was applied to roughly estimate the sliding contact radius a_V and the contact area A_V , as a function of the sliding velocity. Equations (2), (3), and (5) were then fit to the experimental results using l^* , τ_0 , F_0 , τ_f , η_0 and n as fitting parameters. The fits shown in Figs. 2 and 3 were accomplished under the assumption that both the thickness of the sheared hydrogel film δ in Eq. (3) and of the junction d in Eq. (2) are equal to the indentation depth $\delta_{\rm V}$, and hence, a function of load and sliding velocity. It is noteworthy that the thickness of the sheared hydrogel film δ was assumed to be equal to the mesh size previously [24]. However, this assumption did not lead to good results here. The origin for this discrepancy could rely on the greater contact stress and hydrogel deformation in this work, but an accurate comparison to Reference [24] is not possible since the stress at the sliding contact is unknown.

An iterative method using a non-linear solver in MAT-LAB was used to find the best fitting parameters, which required the assumption of appropriate initial values. The fluctuation time of the unconfined polymer, $\tau^{\rm u} = \eta \xi^3/k_{\rm B}T$ (2.3, 1.2, and 0.24 μ s for 4, 6, and 12% hydrogels with ξ equal to 21, 17, and 10 nm, respectively; see SI) gives the lower bound for τ_0 and τ_f , where $\tau_0 \ge \tau_f$. Furthermore, it was found that τ_0 and τ_f influence the increase and the decrease of the adhesive friction with velocity, respectively, while the value of friction at the plateau was strongly sensitive to l*. The initial guess for the stretched length of the polymer bridges before rupture, l^* , was assumed to be the mesh size of the polymer network, ξ . The fit was facilitated by noting that the onset of the velocity-weakening regime is given by $V_{c2} \sim l^*/\tau_f$. A peak in friction was sometimes observed under small applied loads (Fig. 2a), which implies $\tau_0 = \tau_f$. The onset velocity V_{c2} and the peak, when measured, helped to determine the appropriate range of relaxation times. The initial guess for the viscosity was 1 mPas and Newtonian behavior (n=0); these parameters only affected friction at the highest sliding velocities. Due to the large number of



96 Page 8 of 14 Tribology Letters (2018) 66:96

fitting parameters, convergence was not always achieved in Matlab and the fits were then facilitated by manually testing some parameters.

The black lines in Figs. 2a-c and 3a-c show the calculated friction force according to our viscous-adhesive friction model. The fits to the model let us recognize that the behavior of the 12% hydrogel is intrinsically different. This is illustrated in Fig. 5a, which shows representative results for the three hydrogels under an applied load of 40 nN. While 4 and 6% hydrogels exhibit a velocity-weakening adhesive friction (at low sliding velocity), an increase in friction with velocity was reproducibly observed for 12% hydrogels or the same range of sliding velocities. Such increase in friction with velocity cannot be justified by a viscous force with plausible parameters. Instead, the precise logarithmic dependence of friction on velocity (see yellow line in Fig. 5a) suggests the adhesive (elastic) origin of friction in this regime [41]. It should be noted that the distinct behavior of the 12%-hydrogels vanishes when higher compressive stresses are applied with a smaller colloid (Fig. 5b). A comparison between osmotic pressure ($\Pi \sim k_{\rm B}T/\xi^3$, i.e., $\Pi \sim 416, 804, \text{ and } 3340 \text{ Pa for } 4, 6, \text{ and } 12\% \text{ hydrogels},$ respectively) and contact stress supports that fluid drainage might be hindered during the friction-force measurements on 12% hydrogels with the 20-um colloid, while the much higher compressive stress applied with the 5-µm colloid promotes fluid drainage under all investigated conditions. This comparison supports that poroelastic fluid drainage contributes to the observed velocity-weakening frictional behavior. However, the simplified model (Eq. (4)) does not allow a precise evaluation of the poroelastic contribution.

5 Discussion

5.1 Evaluation of the Fitting Parameters

Figure 6a-c shows box diagrams with the fitting parameters for experiments conducted with the 20-µm colloid. The characteristic time of polymer attachment to the colloid (τ_f) was reliably determined only for the hydrogels that clearly exhibited a velocity-weakening adhesive friction at slow sliding velocity. Since this behavior was much less prominent for 12% hydrogels, only a few curves were analyzed in this case. The decrease in $\tau_{\rm f}$ (i.e. shorter time for bond re-formation) with increase in polymer concentration is evident in Fig. 6a, and it indicates that polymer-colloid interactions become more favorable with increase in the polymer concentration. The obtained values for τ_f are at least two orders of magnitude larger than the fluctuation times of the free polymers ($\tau^{\rm u} \sim \eta \xi^3/k_B T$). The large variation of τ_f for the 4% hydrogels is originated by the remarkable effect of the load. Here, it is likely that the more pronounced drainage of the fluid with increasing load favors polymer attachment, which causes τ_f to decrease by two orders of magnitude and to become of the same order of magnitude as that of 6% hydrogels ($\sim 2.10^{-2}$ s). In the limit of high polymer concentration, one could expect $\tau_{\rm f}$ to become so small that the velocity-weakening regime would vanish. This is consistent with the results for 12% hydrogels. In this case, the time of polymer detachment from the colloid τ_0 dictates the friction force, thereby yielding a quasi-logarithmic dependence of friction on velocity (Fig. 3a). Under these conditions, τ_0 is ~ 3(0.8) ×

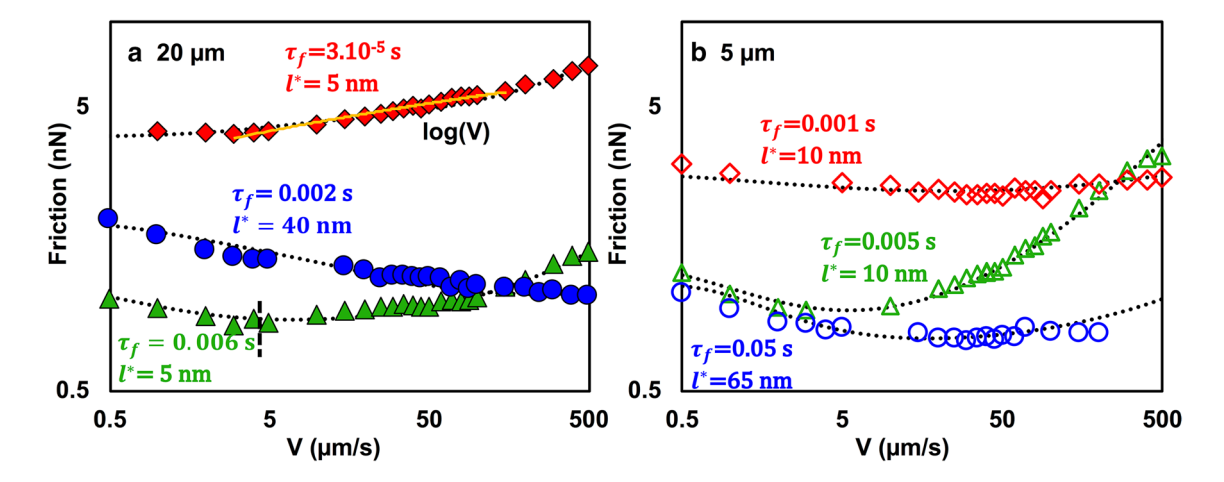


Fig. 5 Comparison of the measured and calculated friction force as a function of the velocity at a normal load of 40 nN for 4% (blue circles), 6% (green triangles), and 12% (red diamonds) hydrogels. The measurements were conducted with **a** the 20- μ m colloid (full symbols) and **b** the 5- μ m colloid (empty symbols). The time required for polymer attachment to the colloid $\tau_{\rm f}$ and the yield length of the

polymer strands l^* are shown in the diagram. The effective viscosity was modeled according to $\eta_{\rm eff} = \eta_0 \left(V/\delta_V\right)^{-0.3}$, with $\eta_0 = 0.01, 0.08$, and $0.36 \, {\rm Pas}/(1/{\rm s})^{-0.3}$ with the 20-µm colloid and $\eta_0 = 0.2, 1.8$, and $0.4 \, {\rm Pas}/(1/{\rm s})^{-0.3}$ with the 5-µm colloid for 4, 6, and 12% hydrogels, respectively. The dashed lines show the fit of the viscous–adhesive friction model to the experimental results. (Color figure online)



Tribology Letters (2018) 66:96 Page 9 of 14 **9**0

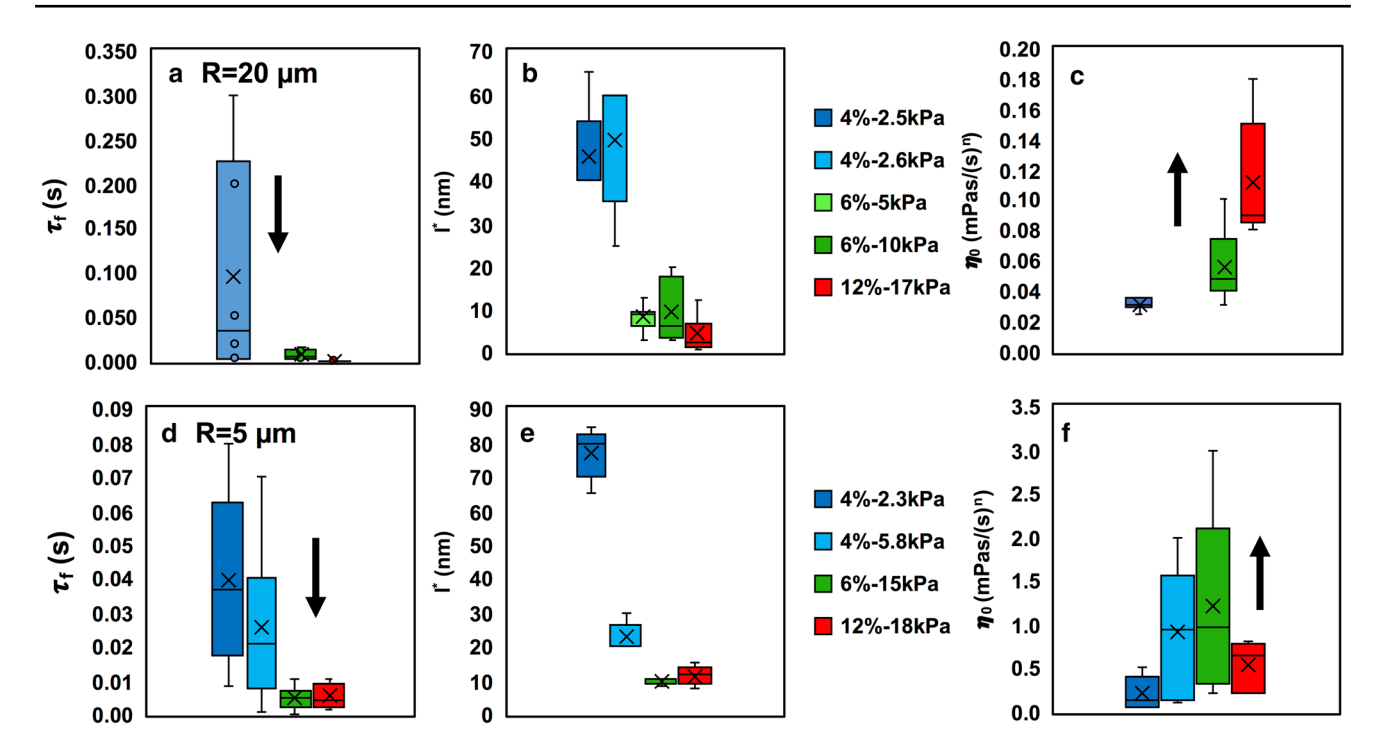


Fig. 6 Box diagrams for **a, d** characteristic time for polymer attachment, τ_f , **b, e** yield length, l^* , and **c, f** viscosity parameter, η_0 , for 4% (blue), 6% (green), and 12% hydrogels (red) with $n \sim -0.3$ (shearthinning behavior), except for 12% hydrogels, where n increased to zero, with **a–c** 20- μ m and **d–f** 5- μ m colloid. The legend in the center shows the corresponding average elastic moduli of the selected hydrogels. The arrow indicates how the fitting parameter changes

with an increase in load. The fitting parameter F_0 is shown in Fig. 8c and d. Assuming that the fluctuation time of the polymer τ^* is given by the fluctuation time of the unconfined polymer, $\tau^u \sim \eta \xi^3/k_{\rm B}$, the activation energies for bond formation $\Delta E_{\rm f}$ can be roughly estimated, yielding 4.6(0.5)kT, 3.7(0.3)kT , and 2.8(0.2)kT for 4, 6, and 12% hydrogels, respectively

 10^{-4} s with a small effect of the load. Under all conditions, it is necessary to consider a velocity-independent term, F_0 , to fit the model to the experimental results, which is discussed in detail later.

At the highest velocities (above the minimum in friction), the viscous dissipation dictates the measured friction force. A non-Newtonian shear-thinning behavior reproduces very well the experimental results using an exponent for the effective viscosity n ranging between -0.3 and -0.35 across all experimental conditions. We emphasize that the use of an effective viscosity is a well-established approximation to account for the viscous dissipation of a viscoelastic material under shear loading [46]. Friction measurements were also conducted with the same colloid on a glass surface in water, for comparison. Figure S4 shows that the dependence of friction with sliding velocity transitions from logarithmic to linear at ~50 µm/s. The linear increase in friction with velocity is attributed to full-fluid film lubrication, where the fluid (water) exhibits a Newtonian behavior, as expected. These reference measurements support that the frictional response at high sliding velocity shown in Figs. 2 and 3 reflects the shear-thinning behavior of the hydrogel. As shown in Fig. 6c, η_0 increases with polymer concentration and with load; the latter is consistent with the squeeze-out of the fluid and a more solid-like behavior of the hydrogel under shear loading. Figure 6d–f shows similar trends of the fitting parameters for the experiments conducted with the 5-µm colloid. However, the viscosity parameter η_0 is about an order of magnitude higher and $\tau_{\rm f}$ is significantly smaller than in Fig. 6a and c, respectively. Both trends may be justified by the larger applied pressures with this colloid, and therefore, more significant fluid drainage and higher polymer concentrations within the contact region.

Figure 6b displays an obvious decrease in the yield length l^* with increase in polymer concentration. The average values ($l^*\sim 50$, 10, and 5 nm for 4, 6, and 12% hydrogels, respectively) correlate well with the mesh size of the hydrogels. Nevertheless, it is worth mentioning that l^* represents the deformation of a junction with length d ($l^*/d\sim$ strain). Since d was assumed to equal the indentation length, the values of l^* might be influenced by this assumption. Our future work will be dedicated to understand better this relation.

We note that although the adhesion energy does not appear as an explicit parameter in this model, it is accounted for in the values of τ_f and τ_0 (characteristic time for bond formation and bond life times) and in the mesh size. Longer bond life times (longest for 4% hydrogels), and smaller relaxation times for re-attachment and mesh size (smallest



96 Page 10 of 14 Tribology Letters (2018) 66:96

for 12% hydrogels) promote adhesion, which is consistent with the maximum in adhesion energy of the 6% hydrogels (Fig. 1b).

5.2 Collapse of the Friction–Velocity Curves into a Master Curve

An inspection of the results in Figs. 2, 3, and S1 shows a transition velocity V^* into a regime where friction is mainly dominated by viscous dissipation. At this transition velocity, a minimum in friction (F_{\min}) is achieved under most of the conditions (except for 12% hydrogels with the 20-µm colloid). Following the practice in our previous work [29], Fig. 7a represents the normalized friction force as a function of the normalized velocity: the Y-axis gives the ratio between the friction force and the minimum friction value F_{\min} , while the X-axis shows the ratio between the sliding velocity and the corresponding transition velocity, V^* . The different colors correspond to the different applied loads with the 20-µm colloid and the different symbols (circles and triangles) are used to distinguish the hydrogel composition (4 and 6% hydrogels). Except for the 12% hydrogels (not shown), which exhibit a velocity-strengthening adhesive friction at slow velocities (Fig. 2c), a good collapse of the normalized friction force is observed. In Fig. 7b, the normalized friction force as a function of the normalized velocity measured with both colloids (with diameters of 5 and 20 µm) is shown together, confirming the good collapse of all the data, also for the 12% hydrogels with the 5-µm colloid. This indicates that the minimum in friction given by F_{\min} and V^* encompasses both the effects of the compressive stress, and hydrogel microstructure, if friction is mainly dictated by a (velocity-weakening) adhesive component and

the concurrent (velocity-strengthening) viscous dissipation. As illustrated in Fig. 7a and b, we find $F/F_{\rm min} \sim (V/V^*)^m$ for most experimental conditions. The exponent m depends on the origin of energy dissipation, thereby changing from $m \sim -0.10$ (adhesive friction) to $m \sim 0.3$ (viscous friction). These exponents are neither sensitive to the contact stress nor to the hydrogel microstructure. As illustrated in Fig. 7, there is a deviation from the proposed power-law for some experiments ($\sim 5-10$ nN, $m \sim 0.5$), which suggests a different molecular mechanism underlying lubrication. We note that Gemini hydrogel interfaces also yield $m \sim 0.5$ [25, 53]. Since this happens at the lowest loads in our experiments, it might be associated with the lack of confinement of the polymer under small loads, but this still requires further investigation.

5.3 Reconciling Previous Models for Hydrogel Friction

In previous works [15, 25, 53], the minimum in friction was related to a critical velocity $V_c \sim \xi/\tau^u \sim k_B T/\eta \xi^2$, at which the fluctuation time of the unconfined polymer τ^u equals the interaction time of the polymer in the sliding contact which is reminiscent of the Deborah number [54]. Other works on polymer friction have, however, proposed that models focused on the relaxation of free polymer chains are not adequate when the polymer is in a confined state [55], as we expect for the hydrogel–colloid interface to some extent, especially when the fluid is drained. In fact, our previous work [29] demonstrated that the experimentally determined V^* was orders of magnitude smaller than V_c . This is not surprising, since the physical concept of the transition velocity V^* significantly differs from V_c . To theoretically demonstrate this, we simplify the viscous–adhesive model assuming a

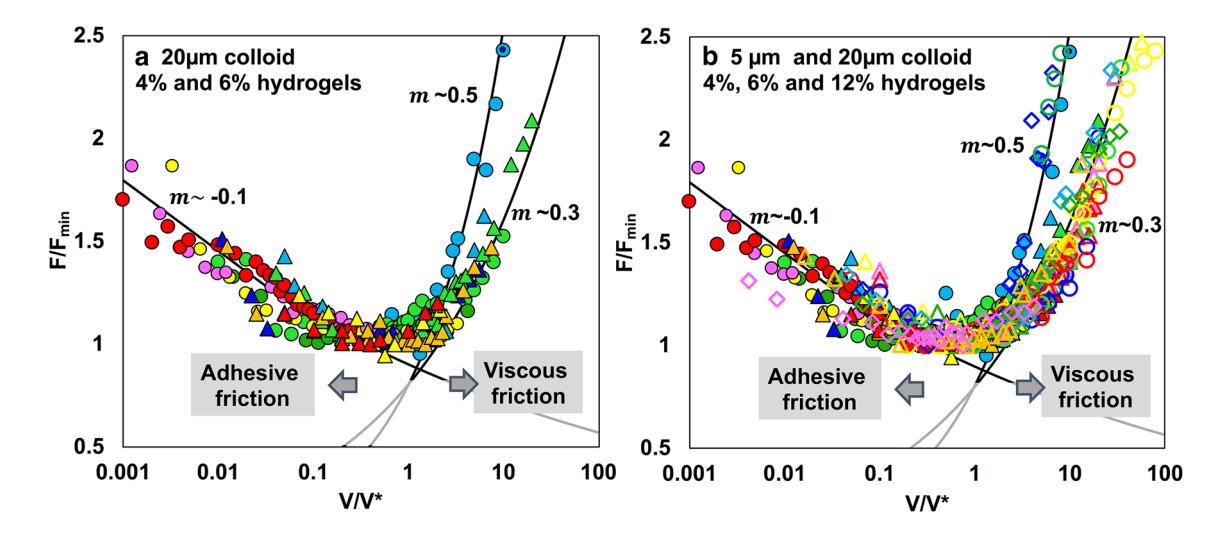


Fig. 7 Normalized friction force $(F/F_{\rm min})$ as a function of the normalized velocity (V/V^*) for 4% (circles), 6% (triangles), and 12% (diamonds) hydrogels measured $\bf a$ with a 20- μ m colloid and $\bf b$ with

20- μ m (full symbols) and 5- μ m (empty symbols) colloids. The black lines give $F/F_{\rm min} \sim (V/V^*)^m$, with $m \sim -0.1$ for the velocity-weakening friction regime and $m \sim +0.3$ to +0.5 for the viscous regime



Tribology Letters (2018) 66:96 Page 11 of 14 **96**

plane–plane geometry and friction only resulting from a velocity-weakening adhesive friction and viscous dissipation, since these two terms are responsible for the observed minimum in friction in our experiments. Under small deformations ($a_{\rm V}^2 \sim R \delta_{\rm V}^2$ and $A_{\rm V} \sim \pi a_{\rm V}^2$) and assuming $\tau_{\rm f} \sim \tau_0$, Eqs. 2–5 can be simplified as follows:

$$F \sim \frac{Gl^*}{2} \frac{A_b}{\delta_V} \left(1 + \frac{l^*}{V \tau_f} \right) + \eta_{\text{eff}} V \frac{A_V}{\delta_V} + F_0$$

$$F \sim \frac{G(l^*)^2}{2V \tau_f} \pi R + \eta_{\text{eff}} V \pi R + F_0$$
(6)

where $\eta_{\rm eff} \sim \eta_0' V^n$ to account for a non-Newtonian behavior; note that the effective viscosity is described here as a function of the velocity and not of the shear strain rate, as in Eq. (3), in order to obtain a simple analytical expression for the derivative of the friction force F. This function achieves a minimum (dF/dV = 0) at the transition velocity V^* :

$$V^* = \left(\frac{Gl^{*2}}{2(1+n)\tau_{\rm f}\eta_0}\right)^{\frac{1}{2+n}} \text{ for } n \geqslant 0, \text{ and } V^* = l^* \left(\frac{G}{2\tau_{\rm f}\eta_0}\right)^{0.5} \text{ for } n = 0$$
(7)

at which the viscous contribution to friction equals the adhesive contribution. Equation (7) only gives a simplified estimation of V^* , and hence, we refrain to quantitatively compare it to our experimental values. Nevertheless, it proves that the transition velocity V^* encompasses the bulk viscoelastic behavior of the hydrogel by means of G, η_0 and n, as well as the relaxation characteristics of the polymer network that determine the interfacial adhesive bonds (l^* and τ_f). We emphasize that the transition velocity V^* arises from the interplay of adhesive and viscous friction, while the critical velocity V_c (in previous works) only refers to the relaxation behavior of the polymer network. This suggests that the viscous dissipation hinders V_c to be experimentally attained.

Figure 8a, b shows the experimentally determined transition velocity V^* for the three hydrogels. Equation (7) can qualitatively explain the convoluted influence of hydrogel viscoelasticity, interfacial properties, and stress on V^* : hydrogels with higher polymer concentration and crosslinking degree have both a higher shear modulus and effective viscosity, and shorter relaxation length l^* and time τ_f . As shown in Fig. 6, the viscosity and relaxation times were found to change with load in an opposite fashion, which is then reflected in the complex variation of V^* with load. When using the 20-um colloid (Fig. 8), the viscosity increase with load seems to predominantly affect 6% hydrogels, thereby causing V^* to decrease with an increase in load; while in 4% hydrogels, the decrease of the relaxation time with load seems more relevant, especially at high loads, since V^* increases with an increase in load. When using the 5- μ m colloid, i.e., at higher contact stresses and more pronounced squeeze-out of water, the change in viscosity with load seems to dictate the variation of V^* for 4 and 6% hydrogels, while the effect of the relaxation time appears more prominent for the 12% hydrogels, perhaps because it is so small. Figure 8b suggests that, at the highest contact stresses, the transition into viscous dissipation is delayed for hydrogels with higher polymer concentration and crosslinking degree (smaller mesh size).

Combining Eqs. (6) and (7), the minimum in friction is given by $F_{\min} = F_0 + l^* \pi R \sqrt{G \eta_0 / 2\tau_f}$ for n=0; a similar expression is obtained for shear thinning that we do not show here for simplicity. A collapse of the normalized friction (F/F_{\min}) versus normalized velocity (V/V^*) is only possible if the static friction is given by

$$F_0 = k l^* \pi R \sqrt{\frac{G\eta_0}{2\tau_{\rm f}}} \tag{8}$$

and therefore, $F_{\min} = (k+1) F_0$, k being a constant. This has been obtained in the limit of small deformations, $A_{\rm V}/\delta_{\rm V} \sim \pi R$, and assuming $\tau_{\rm f} \sim \tau_0$, a plane–plane geometry and Newtonian behavior. Although deviations from these expressions are obviously expected for the experimentally investigated hydrogels, Fig. 8c and d confirm the correlation between F_0 (fitting parameter) and F_{\min} (minimum friction force) in experiments, implying that the minimum friction force is limited by F_0 . Nevertheless, this relation still requires more systematic studies. Importantly, F_{\min} is similar for 4 and 6% hydrogels, which seems to result from the balance between adhesive and viscous friction (viscous friction is greater for 6% hydrogels than for 4% hydrogels, while the opposite is observed for the adhesive friction) but F_{\min} is much greater for 12% hydrogels. In summary, there is a complex interplay between hydrogel's microstructure and adhesive and viscous frictional dissipation.

5.4 Implications

The discussed results indicate that efficient hydrogel lubrication is dictated by the convolution of bulk and interfacial properties and it depends on the loading conditions. Despite the simplicity of the proposed model, it enables to correlate the hydrogel's microstructure to the frictional response through physically based parameters, and it helps to predict the hydrogel's frictional response under different loading conditions in the absence of wear.

Furthermore, the described model can inspire design strategies that afford control of the velocity-weakening frictional response. For instance, a less crosslinked surface layer supported by a more crosslinked (stiffer) hydrogel appears as a design approach to increase V^* according to Eq. (7),



96 Page 12 of 14 Tribology Letters (2018) 66:96

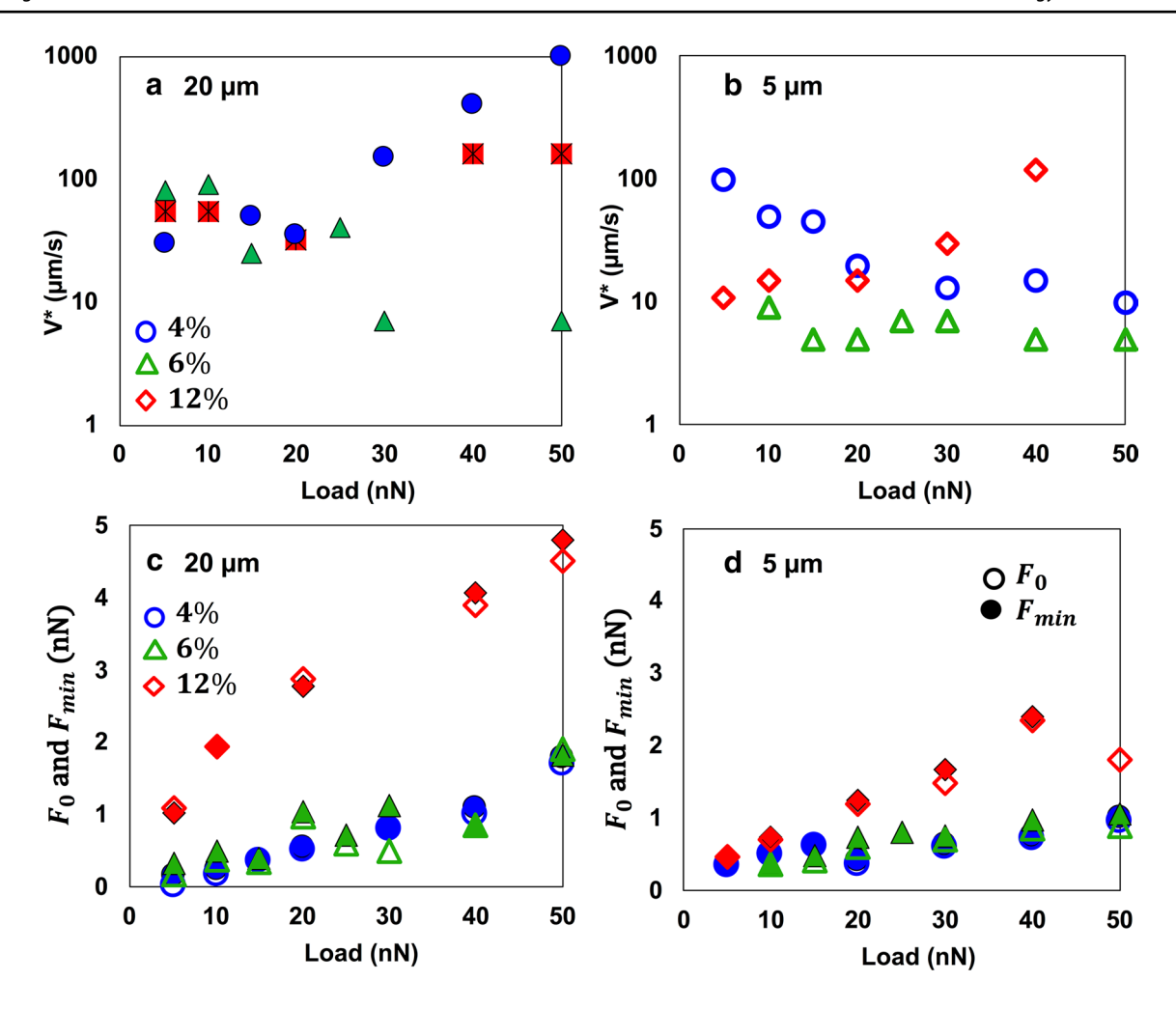


Fig. 8 a, b Transition velocity V^* , **c, d** friction minimum F_{\min} (full symbols) and static friction F_0 (empty symbols) as a function of load for 4, 6, and 12% hydrogels, measured with the **a–c** 20- μ m colloid and **b–d** 5- μ m colloid for the experiments shown in Figs. 2 and 3. The transition velocity V^* for 12% hydrogels with the 20- μ m colloid

has been also depicted (red squares with stars in **a**), even if a minimum was not attained at V^* in this case. Estimated $V_c = k_{\rm B}T/\eta\xi^2$ yields 9.3, 14, 41 mm/s for 4, 6, and 12% hydrogels with ξ equal to 21, 17, and 10 nm, respectively

and therefore, to shift the viscous dissipation to higher sliding velocities. As a matter of fact, biological systems that are characterized by very low coefficients of friction exhibit graded microstructures. Mucins, which are gel-forming, high molecular weight glycosylated proteins, are present in the inner most layer of the tear film on the surface of the cornea to provide protection, hydration, and lubrication during regular eye functions [56, 57]. Similarly, glycoproteins with bottle-brush structures adsorb on the surface of (poroelastic) cartilage and help to reduce friction [58, 59]. Synthetic approaches have already proved the efficiency of this relation. For instance, the surface functionalization of PDMS [60] and (pHEMA) hydrogels [26] with polymer brushes and entangled polymer networks have shown a decrease in friction coefficient by orders of magnitude while retaining the structural integrity of the system. Along the same lines,

contact lenses exhibit a graded microstructure with surface layers that have a lower elastic modulus and higher water contents compared to the core material [5].

Interestingly, our experimental results (Fig. 7) show a prominent plateau around the friction minimum (instead of a sharp minimum), perhaps arising from the shear-thinning behavior of the hydrogels. The focus of our ongoing work is to provide a better understanding of the viscous energy dissipation by scrutinizing the nanorheological response of the hydrogel's near-surface region. New design strategies of hydrogel-based materials with a high load-bearing capacity, along with high lubricity via the control of the viscous dissipation (for instance, through the extension of this plateau over a wider range of sliding velocities), could emerge from our current and future research.



Tribology Letters (2018) 66:96 Page 13 of 14 **9**

6 Conclusions

This work has shown a non-monotonic frictional behavior for PAAm hydrogels with three different compositions that were scrutinized in the light of a viscous-adhesive friction model. The model accounts for the formation of thermally activated transient (adhesive) bonds between the polymer and the counter-surface and the shear-thinning rheology of the hydrogel. In contrast to previous models for hydrogel friction, the proposed approach accounts for the effect of contact stresses on the fluctuation characteristics of the polymer network. Using this model, we obtain a theoretical, yet simplified, expression for V^* , which defines the transition from adhesive to viscous dissipation. The transition velocity accounts for the hydrogel's viscoelasticity by means of two parameters, i.e., G and η , as well as for the relaxation (length and time) characteristics of the polymer at the interface. The transition velocity, V^* , and the minimum in friction, F_{\min} , encompass the influence of the microstructure and of the load on friction, and they help to define a master curve $F/F_{\min} \sim (V/V^*)^m$. The exponent m considers the mechanism of energy dissipation for most of the experimental conditions: m = -0.1 for the energy dissipated in breaking the adhesive bonds across the interface, thereby yielding a velocity-weakening (adhesive) friction force and m = 0.3 for viscous dissipation, which leads to an increase in friction with sliding velocity above V^* . A deviation from this behavior is observed in our experiments with 12% hydrogels, which can exhibit a velocity-strengthening (adhesive) friction force, thereby emphasizing the relevance of the poroelastic behavior of hydrogels in their frictional behavior. Our work shows a complex interrelation between hydrogel's microstructure and the mechanisms underlying hydrogel lubrication and highlights the associated challenges in the design of soft systems with extremely low friction.

Acknowledgements Support to TS by the Fulbright Program, U.S. Department, of State is acknowledged. This material is based upon work supported by the National Science Foundation under Grant No. CMMI-17-61696.

References

- Dowson, D.: Bio-tribology. Faraday Discuss. 156, 9–30 (2012). https://doi.org/10.1039/c2fd20103h.
- Sterner, O., Karageorgaki, C., Zurcher, M., Zurcher, S., Scales, C.W., Fadli, Z., Spencer, N.D., Tosatti, S.G.P.: Reducing friction in the eye: a comparative study of lubrication by surface-anchored synthetic and natural ocular mucin analogues. ACS Appl. Mater. Interfaces. 9(23), 20150–20160 (2017). https://doi.org/10.1021/ acsami.6b16425
- Pult, H., Tosatti, S.G., Spencer, N.D., Asfour, J.M., Ebenhoch, M., Murphy, P.J.: Spontaneous blinking from a tribological viewpoint. Ocul. Surf. 13(3), 236–249 (2015). https://doi.org/10.1016/j. jtos.2014.12.004

- Samsom, M., Chan, A., Iwabuchi, Y., Subbaraman, L., Jones, L., Schmidt, T.A.: In vitro friction testing of contact lenses and human ocular tissues: effect of proteoglycan 4 (PRG4). Tribol. Int. 89, 27–33 (2015). https://doi.org/10.1016/j.triboint.2014.11.022
- Dunn, A.C., Urueña, J.M., Puig, E., Perez, V.L., Sawyer, W.G.: Friction coefficient measurement of an in vivo murine cornea. Tribol. Lett. 49(1), 145–149 (2012). https://doi.org/10.1007/s1124 9-012-0033-6
- Dunn, A.C., Cobb, J.A., Kantzios, A.N., Lee, S.J., Sarntinoranont, M., Tran-Son-Tay, R., Sawyer, W.G.: Friction coefficient measurement of hydrogel materials on living epithelial cells. Tribol. Lett. 30(1), 13–19 (2008). https://doi.org/10.1007/s11249-008-9306-5
- Faust, T.: Coordination driven gelation. Nat. Chem. 7(9), 681–681 (2015). https://doi.org/10.1038/nchem.2339
- Pan, Y., Xiong, D.: Friction properties of nano-hydroxyapatite reinforced poly(vinyl alcohol) gel composites as an articular cartilage. Wear. 266(7–8), 699–703 (2009). https://doi.org/10.1016/j. wear.2008.08.012
- Gong, J., Iwasaki, Y., Osada, Y., Kurihara, K., Hamai, Y.: Friction of gels. 3. Friction on solid surfaces. J. Phys. Chem. B. 103(29), 6001–6006 (1999). https://doi.org/10.1021/jp9902553
- Chang, D.P., Dolbow, J.E., Zauscher, S.: Switchable friction of stimulus-responsive hydrogels. Langmuir. 23(1), 250–257 (2007). https://doi.org/10.1021/la0617006
- Pan, Y.-S., Xiong, D.-S., Ma, R.-Y.: A study on the friction properties of poly(vinyl alcohol) hydrogel as articular cartilage against titanium alloy. Wear. 262(7–8), 1021–1025 (2007). https://doi.org/10.1016/j.wear.2006.10.005
- Kim, S.H., Opdahl, A., Marmo, C., Somorjai, G.A.: AFM and SFG studies of pHEMA-based hydrogel contact lens surfaces in saline solution: adhesion, friction, and the presence of non-crosslinked polymer chains at the surface. Biomaterials. 23(7), 1657–1666 (2002). https://doi.org/10.1016/s0142-9612(01)00292-7
- Reale, E.R., Dunn, A.C.: Poroelasticity-driven lubrication in hydrogel interfaces. Soft Matter. 13(2), 428–435 (2017). https:// doi.org/10.1039/c6sm02111e
- Gong, J., Osada, Y.: Gel friction: A model based on surface repulsion and adsorption. J. Chem. Phys. 109(18), 8062–8068 (1998). https://doi.org/10.1063/1.477453
- Kurokawa, T., Tominaga, T., Katsuyama, Y., Kuwabara, R., Furukawa, H., Osada, Y., Gong, J.P.: Elastic-hydrodynamic transition of gel friction. Langmuir. 21(19), 8643–8648 (2005). https://doi. org/10.1021/la050635h
- Kagata, G., Gong, J.P., Osada, Y.: Friction of gels. 6. Effects of sliding velocity and viscoelastic responses of the network. J. Phys. Chem. B. 106(18), 4596–4601 (2002). https://doi.org/10.1021/ jp012380w
- Ohsedo, Y., Takashina, R., Gong, J.P., Osada, Y.: Surface friction of hydrogels with well-defined polyelectrolyte brushes. Langmuir 20(16), 6549–6555 (2004). https://doi.org/10.1021/la036211&%23x002B;
- Schallamach, A.: A theory of dynamic rubber friction. Wear. 6(5), 375–382 (1963). https://doi.org/10.1016/0043-1648(63)90206-0
- Gong, J.P.: Friction and lubrication of hydrogels—its richness and complexity. Soft Matter. 2(7), 544–552 (2006). https://doi. org/10.1039/b603209p
- Li, A., Ramakrishna, S.N., Kooij, E.S., Espinosa-Marzal, R.M., Spencer, N.D.: Poly(acrylamide) films at the solvent-induced glass transition: adhesion, tribology, and the influence of crosslinking. Soft Matter. 8(35), 9092–9100 (2012). https://doi.org/10.1039/ c2sm26222c
- Kim, S.H., Marmo, C., Somorjai, G.A.: Friction studies of hydrogel contact lenses using AFM: non-crosslinked polymers of low friction at the surface. Biomaterials. 22(24), 3285–3294 (2001). https://doi.org/10.1016/s0142-9612(01)00175-2



96 Page 14 of 14 Tribology Letters (2018) 66:96

- Li, A., Benetti, E.M., Tranchida, D., Clasohm, J.N., Schönherr, H., Spencer, N.D.: Surface-grafted, covalently cross-linked hydrogel brushes with tunable interfacial and bulk properties. Macromolecules. 44(13), 5344–5351 (2011). https://doi.org/10.1021/ma200 6443
- Gong, J.P., Kurokawa, T., Narita, T., Kagata, G., Osada, Y., Nishimura, G., Kinjo, M.: Synthesis of hydrogels with extremely low surface friction. J. Am. Chem. Soc.. 123(23), 5582–5583 (2001). https://doi.org/10.1021/ja003794q
- Baumberger, T., Caroli, C., Ronsin, O.: Self-healing slip pulses and the friction of gelatin gels. Eur. Phys. J. E. 11(1), 85–93 (2003). https://doi.org/10.1140/epje/i2003-10009-7
- Urueña, J.M., Pitenis, A.A., Nixon, R.M., Schulze, K.D., Angelini, T.E., Sawyer, W.G.: Mesh size control of polymer fluctuation lubrication in gemini hydrogels. Biotribology. 1–2, 24–29 (2015). https://doi.org/10.1016/j.biotri.2015.03.001
- Pitenis, A.A., Manuel Urueña, J., Nixon, R.M., Bhattacharjee, T., Krick, B.A., Dunn, A.C., Angelini, T.E., Sawyer, G.: W.: Lubricity from entangled polymer networks on hydrogels. J. Tribol. 138(4), 042102 (2016). https://doi.org/10.1115/1.4032889
- Sokoloff, J.B.: Theory of hydrostatic lubrication for two likecharge polymer hydrogel coated surfaces. Soft Matter 6(16) (2010). https://doi.org/10.1039/c000252f
- Gong, J.P., Kagata, G., Osada, Y.: Friction of gels. 4. Friction on charged gels. J. Phys. Chem. B 103(29), 6007–6014 (1999)
- Shoaib, T., Heintz, J., Lopez-Berganza, J.A., Muro-Barrios, R., Egner, S.A., Espinosa-Marzal, R.M.: Stick-slip friction reveals hydrogel lubrication mechanisms. Langmuir. 34(3), 756–765 (2018). https://doi.org/10.1021/acs.langmuir.7b02834
- Grosch, K.A.: The relation between the friction and visco-elastic properties of rubber. Proc. Royal Soc. A. 274(1356), 21–39 (1963). https://doi.org/10.1098/rspa.1963.0112
- 31. Rennie, A.C., Dickrell, P.L., Sawyer, W.G.: Friction coefficient of soft contact lenses: measurements and modeling. Tribol. Lett. **18**(4), 499–504 (2005)
- Baumberger, T., Caroli, C., Ronsin, O.: Self-healing slip pulses along a gel/glass interface. Phys. Rev. Lett. 88(7), 075509 (2002). https://doi.org/10.1103/PhysRevLett.88.075509
- Tse, J.R., Engler, A.J.: Preparation of hydrogel substrates with tunable mechanical properties. Current Protocols in Cell Biology Chap. 10, Unit. 10 16 (2010). https://doi.org/10.1002/0471143030. cb1016s47
- Cannara, R.J., Eglin, M., Carpick, R.W.: Lateral force calibration in atomic force microscopy: a new lateral force calibration method and general guidelines for optimization. Rev. Sci. Instrum. 77(5), 053701 (2006)
- Pabst, W., Gregorová, E.V.A.: Elastic properties of silica polymorphs—a review. Ceram. Silik. 57(3), 167–184 (2013)
- Hertz, H.: Über die Berührung fester elastischer Körper. Reine Angewandte Mathematik 92, 156–171 (1881)
- Ramakrishna, S.N., Cirelli, M., Divandari, M., Benetti, E.M.: Effects of lateral deformation by thermoresponsive polymer brushes on the measured friction forces. Langmuir. 33(17), 4164– 4171 (2017). https://doi.org/10.1021/acs.langmuir.7b00217
- Gautreau, Z., Griffin, J., Peterson, T., Thongpradit, P.: Characterizing viscoelastic properties of polyacrylamide gels. Worcester Polytechnic Institute, Worcester (2006)
- Resnikoff, J.I.N.: The role of extracellular matrix composition and mechanical properties in driving cardiac differentiation of mesenchymal stem cells. (2012)
- Schallamach, A.: How does rubber slide? Wear 17(4), 301–312 (1971)
- Drummond, C., Israelachvili, J., Richetti, P.: Friction between two weakly adhering boundary lubricated surfaces in water. Phys. Rev. E. 67(6 Pt 2), 066110 (2003). https://doi.org/10.1103/PhysR evE.67.066110

- Dhinojwala, A., Cai, L., Granick, S.: Critique of the friction coefficient concept for wet (lubricated) sliding. Langmuir 12(19), 4537–4542 (1996)
- Demirci, U., Khademhosseini, A.: Gels handbook: Fundamentals, properties and applications (in 3 volumes). World scientific, (2016)
- 44. Rubinstein, M., Colby, R.H.: Polymer Physics. OUP, Oxford (2003)
- 45. Savkoor, A.R.: On the friction of rubber. Wear. **8**(3), 222–237 (1965). https://doi.org/10.1016/0043-1648(65)90161-4
- Luengo, G., Schmitt, F.-J., Hill, R., Israelachvili, J.: Thin film rheology and tribology of confined polymer melts: contrasts with bulk properties. Macromolecules. 30(8), 2482–2494 (1997). https://doi.org/10.1021/ma9519122
- Schulze, K.D., Hart, S.M., Marshall, S.L., O'Bryan, C.S., Urueña, J.M., Pitenis, A.A., Sawyer, W.G., Angelini, T.E.: Polymer osmotic pressure in hydrogel contact mechanics. Biotribology. 11, 3–7 (2017). https://doi.org/10.1016/j.biotri.2017.03.004
- 48. Mow, V.C., Kuei, S.C., Lai, W.M., Armstrong, C.G.: Biphasic creep and stress relaxation of articular cartilage in compression? Theory and experiments. J. Biomech. Eng. **102**(1), 73–84 (1980). https://doi.org/10.1115/1.3138202
- Strange, D.G.T., Fletcher, T.L., Tonsomboon, K., Brawn, H., Zhao, X., Oyen, M.L.: Separating poroviscoelastic deformation mechanisms in hydrogels. Appl. Phys. Lett. 102(3), 031913 (2013). https://doi.org/10.1063/1.4789368
- Espinosa-Marzal, R.M., Bielecki, R.M., Spencer, N.D.: Understanding the role of viscous solvent confinement in the tribological behavior of polymer brushes: a bioinspired approach. Soft Matter 9(44), 10572–10585 (2013)
- Johnson, K.L., Kendall, K., Roberts, A.D.: Surface energy and the contact of elastic solids. Proc. R. Soc. Lond. A 324, 301–313
- Suriano, R., Griffini, G., Chiari, M., Levi, M., Turri, S.: Rheological and mechanical behavior of polyacrylamide hydrogels chemically crosslinked with allyl agarose for two-dimensional gel electrophoresis. J. Mech. Behav. Biomed. Mater. 30, 339–346 (2014). https://doi.org/10.1016/j.jmbbm.2013.12.006
- Pitenis, A.A., Uruena, J.M., Schulze, K.D., Nixon, R.M., Dunn, A.C., Krick, B.A., Sawyer, W.G., Angelini, T.E.: Polymer fluctuation lubrication in hydrogel gemini interfaces. Soft Matter. 10(44), 8955–8962 (2014). https://doi.org/10.1039/c4sm01728e
- 54. Reiner, M.: The deborah number. Phys. today 17(1), 62 (1964)
- Persson, B.N., Volokitin, A.I.: Rubber friction on smooth surfaces. Eur. Phys. J. E. 21(1), 69–80 (2006). https://doi.org/10.1140/epje/ i2006_10045_9
- Hodges, R.R., Dartt, D.A.: Tear film mucins: front line defenders of the ocular surface; comparison with airway and gastrointestinal tract mucins. Exp. Eye Res. 117, 62–78 (2013). https://doi. org/10.1016/j.exer.2013.07.027
- Bansil, R., Turner, B.S.: Mucin structure, aggregation, physiological functions and biomedical applications. Curr. Opin. Colloid Interface Sci. 11(2–3), 164–170 (2006). https://doi.org/10.1016/j.cocis.2005.11.001
- Jay, G.D., Waller, K.A.: The biology of lubricin: near frictionless joint motion. Matrix Biol. 39, 17–24 (2014). https://doi. org/10.1016/j.matbio.2014.08.008
- Swann, D.A., Slayter, H.S., Silver, F.H.: The molecular structure of lubricating glycoprotein-I, the boundary lubricant for articular cartilage. J. Biol. Chem. 256(11), 5921–5925 (1981)
- Chawla, K., Lee, S., Lee, B.P., Dalsin, J.L., Messersmith, P.B., Spencer, N.D.: A novel low-friction surface for biomedical applications: modification of poly(dimethylsiloxane) (PDMS) with polyethylene glycol(PEG)-DOPA-lysine. J. Biomed. Mater. Research A. 90(3), 742–749 (2009). https://doi.org/10.1002/jbm.a.32141

